Reaction of H_2 and H_2S with $CoMoO_4$ and $NiMoO_4$: TPR, XANES, Time-Resolved XRD, and Molecular-Orbital Studies

José A. Rodriguez,* Sanjay Chaturvedi, and Jonathan C. Hanson

Department of Chemistry, Brookhaven National Laboratory, Upton, New York 11973

Joaquín L. Brito*

Centro de Química, Instituto Venezolano de Investigaciones Científicas (IVIC), Apartado 21827, Caracas 1020-A, Venezuela

Received: July 22, 1998; In Final Form: October 22, 1998

The combination of two metals in an oxide matrix can produce materials with novel physical and chemical properties. The reactivity of a series of cobalt and nickel molybdates (α-$AMoO_4$, β-$AMoO_4$, and $AMoO_4 \cdot nH_2O$; A = Co or Ni) toward H_2 and H_2S was examined using temperature programmed reduction (TPR), synchrotron-based X-ray powder diffraction (XRD), and X-ray absorption near-edge spectroscopy (XANES). In general, the cobalt and nickel molybdates are more reactive toward H_2 and easier to reduce than pure molybdenum oxides: $MoO_2 < MoO_3 < CoMoO_4 < NiMoO_4$. The interaction of H_2 with surfaces of α-$NiMoO_4$, α-$CoMoO_4$, and α-MoO_3 was investigated using ab initio SCF calculations and cluster models. The mixed-metal oxides are easier to reduce due to the combination of two factors. First, it is easier to adsorb and dissociate H_2 on Ni or Co sites than on Mo sites of an oxide. And second, as a result of differences in the strength of the metal−oxygen bonds, it is easier to remove oxygen as water from the nickel and cobalt molybdates than from MoO_3 or MoO_2. The extra reactivity that the Co and Ni atoms provide also makes the rate of sulfidation of the cobalt and nickel molybdates faster than that of pure molybdenum oxides. For the adsorption of H_2S, HS, and S on α-$NiMoO_4$ and α-MoO_3 clusters, the results of ab initio SCF calculations show bigger bonding energies on the Ni sites than on the Mo sites. In these systems, the oxidation state of the Ni atoms is substantially lower (i.e., larger electron density) than that of the Mo atoms, favoring the formation of Ni → SH and Ni → S dative bonds. The behavior of the cobalt and nickel molybdates is a very good example of how one can enhance the chemical activity of an oxide (MoO_3) by adding a second metal cation to the system. Results of time-resolved XRD and XANES indicate that the reduced $AMoO_4$ compounds can be regenerated by reaction with O_2 at high temperatures (350−450 °C). A similar procedure ($S_a + O_{2,gas} \rightarrow SO_{2,gas}$) can be used to remove most of the sulfur from the sulfided oxides.

I. Introduction

Metal oxides are used as catalysts in a large variety of commercial processes that involve the conversion of hydrocarbons.[1,2] Selective oxidation, ammoxidation, and selective dehydrogenation probably constitute the most important catalytic uses of transition metal oxides.[1] Recently, much attention has been focused on the preparation and performance of mixed metal−oxide catalysts.[2b−4] In principle, the combination of two metals in an oxide matrix can produce materials with novel structural or electronic properties that can lead to superior catalytic activity or selectivity. In simple terms, the two metals centers can work in a cooperative way catalyzing different steps of a chemical process, or they can have an enhanced chemical activity due to the effects of metal:metal or metal:oxygen:metal interactions.[2b−4] One of the metals may be simply seen (or classified) as a "promoter" of catalytic activity.[2b] Bimetallic oxides usually can adopt several crystal structures or phases depending on the composition and temperature of the system,[5,6] and in many cases these phases exhibit distinct chemical and catalytic properties.[2b−4,7−10] Thus, when working with this type of system, one has several variables that could be adjusted to improve the performance of the catalyst. To do this, a fundamental and general understanding of the chemical behavior of bimetallic oxides is necessary.[1−4]

Cobalt and nickel molybdates are important components of industrial catalysts for the partial oxidation of hydrocarbons[11] and precursors in the synthesis of hydrodesulfurization (HDS) catalysts.[9,10,12,13] In general, these molybdates can be seen as the product of adding CoO or NiO to MoO_3. Under atmospheric pressure, three compounds of $AMoO_4$ stoichiometry (A = Co or Ni) are known: the low temperature α-phase, the high temperature β-isomorph, and the hydrate (α-$AMoO_4$, β-$AMoO_4$, and $AMoO_4 \cdot nH_2O$, respectively).[14,15] The catalytic properties of the cobalt and nickel molybdates are closely related to their structures.[8−10] The β-phase of $NiMoO_4$ is almost twice as selective for the dehydrogenation of propane to propene than the α-phase.[8] In a series of studies,[9,10,16] the sulfided H_2O−$CoMoO_4$ and H_2O−$NiMoO_4$ compounds were found to be much better catalysts for the HDS of thiophene than the corresponding sulfided α- and β-isomorphs. The HDS activity of these systems increased in the following order:[10] $\alpha < \beta <$ hydrate.

In the cobalt and nickel molybdates, Co and Ni are in octahedral sites in all the isomorphs, whereas the coordination of Mo varies from octahedral in the α-phases to tetrahedral in

* Corresponding authors.

10.1021/jp983115m CCC: $18.00
Published on Web 01/20/1999

the β-phases and hydrates.[14,15] Upon heating of $AMoO_4 \cdot nH_2O$, evolution of water is seen at two different temperature ranges: 100−200 °C for reversibly bound H_2O; 200−400 °C for H_2O from the crystal structure.[15] The results of time-resolved synchrotron-based X-ray powder diffraction (XRD) show a direct transformation of the hydrates into the β-$AMoO_4$ compounds (following a kinetics of first order) without any intermediate phase.[15] This is probably facilitated by the similarities that $AMoO_4 \cdot nH_2O$ and β-$AMoO_4$ have in their structural and electronic properties.[15] The XRD experiments show that the α-$AMoO_4 \rightarrow \beta$-$AMoO_4$ transitions occur at much higher temperatures than the hydrate $\rightarrow \beta$-$AMoO_4$ transformations ($\Delta T \approx 150$ °C in $CoMoO_4$ and 280 °C in $NiMoO_4$). The activation energy for the α-$NiMoO_4 \rightarrow \beta$-$NiMoO_4$ transition is $\sim$ 40 kcal/mol larger than that for the $NiMoO_4 \cdot nH_2O \rightarrow \beta$-$NiMoO_4 + nH_2O$ reaction.[15] The larger activation energy reflects the change in the coordination of Mo ($O_h \rightarrow T_d$) that occurs during the $\alpha \rightarrow \beta$ transition.

In the $AMoO_4$ and $AMoO_4 \cdot nH_2O$ compounds, the formal oxidation state of Co and Ni is +2, whereas that of Mo is +6 as in MoO_3. The K- and L-edges of Co in X-ray absorption near-edge spectroscopy (XANES) indicate that there are no large variations in the electronic properties of this metal when comparing $CoMoO_4 \cdot nH_2O$, α-$CoMoO_4$, and β-$CoMoO_4$.[15] The same is valid for the electronic properties of Ni in the nickel molybdates. In contrast, the $L_{II,III}$-edges of Mo show large changes in the splitting of the Mo 4d orbitals as the coordination of this metal varies from octahedral (α-phases) to tetrahedral (β-phases and hydrates).[15] In the α-$AMoO_4$ and MoO_3 oxides, the Mo atoms are in an octahedral environment and have similar electronic properties.[15]

In many applications the cobalt and nickel molybdates are prereduced with hydrogen or sulfided with H_2S in order to enhance their catalytic activities.[9−11] In this article, we investigate the reactions of H_2 and H_2S with the $CoMoO_4$ and $NiMoO_4$ compounds using temperature programmed reduction (TPR), synchrotron-based XANES, and ab initio self-consistent-field (SCF) calculations. The reoxidation of the reduced and sulfided molybdates is studied using time-resolved synchrotron XRD and XANES. One of our objectives is to compare the chemical reactivity of the bimetallic oxides with that of pure molybdenum oxides, systems that have well-known catalytic properties.[1,2]

II. Experimental and Theoretical Methods

II.1. Preparation of the Molybdates. The $H_2O-AMoO_4$ and $AMoO_4$ samples were prepared following the methodology described in ref 10. Hydrated compounds of general formula $AMoO_4 \cdot nH_2O$ were synthesized by coprecipitation from aqueous solution of A^{2+} salts (nickel and cobalt nitrates) and ammonium heptamolybdate.[10,17] The α and β isomorphs of $NiMoO_4$ were prepared by heating the $NiMoO_4 \cdot nH_2O$ hydrate to 550 °C and subsequent cooling to 300 °C (β-$NiMoO_4$) or room temperature (α-$NiMoO_4$).[15] The β-$CoMoO_4$ isomorph was prepared by calcining the $CoMoO_4 \cdot nH_2O$ precursor at 550 °C, followed by fast cooling (−100 °C/min) to room temperature. The β-phase of the cobalt molybdate is stable at 25 °C, and the grinding of this compound is necessary in order to produce the corresponding α-phase.[10]

II.2. Reduction and Sulfidation of the Molybdates. The H_2-TPR experiments were done in a RXM-100 instrument from Advanced Scientific Designs. The samples were put in the reaction cell under a 15% H_2/85% N_2 mixture (flow rate = 50 cm^3/min) and the temperature was ramped from 40 to 600 °C at a heating rate of 20 °C/min. The consumption of H_2 and evolution of H_2O were monitored using a quadrupole mass spectrometer (UTI 100C).

The $AMoO_4$ and $AMoO_4 \cdot nH_2O$ samples were partially sulfided by exposing them to a 10%H_2S/90%He mixture at 400 °C in a U tube quartz reactor.

II.3. X-ray Absorption Near-Edge Spectroscopy. The O K-edge XANES spectra of the pure, reduced, and sulfided samples were collected at the national synchrotron light source (NSLS) using the U7A beam line. This beam line is equipped with a toroidal−spherical grating monochromator.[18] The energy resolution at the O K-edge was close to 0.3 eV. All the O K-edge spectra were acquired at room temperature in the "electron-yield mode".[18]

The S K-edge spectra of the sulfided $AMoO_4$ and $AMoO_4 \cdot nH_2O$ samples were collected on beam line X19A of the NSLS. The X-ray photons were monochromatized using a NSLS boomerang-type flat crystal monochromator with Si(111) crystals. The energy resolution was $\sim$ 0.5 eV. The S K-edge spectra were recorded at room temperature in the "fluorescence-yield mode" using a Stern-Heald-Lytle detector with argon as the detector gas.[15]

II.4. Time-Resolved X-ray Powder Diffraction. The time-resolved diffraction data were collected on beam line X7B of the NSLS.[19] The sample was kept in a quarz capillary and heated using a small resistance heater placed under the capillary.[15,20] A chromel−alumel thermocouple was used to measure the temperature of the sample. The accuracy of the thermocouple readings was verified by doing blank runs with silver powder and checking against the known changes in the cell parameters of this metal as a function of temperature.[20] Data collections were performed using a wavelength of 1.004 Å. The X-ray powder diffraction patterns were accumulated on a flat image plate (IP) detector. In this experimental setup, a continuous set of powder patterns can be obtained as a function of time or temperature.[20] The images collected on the IP were retrieved using a Fuji BAS2000 scanner.

II.5. Molecular-Orbital Calculations. The ab initio SCF calculations described in sections III.1. and III.2. were performed using the HONDO program.[21] Surfaces of $NiMoO_4$, $CoMoO_4$, and MoO_3 are modeled using clusters of medium size (17−19 atoms). Since these systems contain a large number of heavy atoms, the use of all-electron wave functions is not practical from a computational viewpoint. The nonempirical effective core potentials (ECPs) of Hay and Wadt[22] were used to describe the inner shells of the metals (Co, Ni, Mo), while the 1s shell of O was described through the ECP generated by Stevens, Basch, and Krauss.[23] In the past, we have found that the use of effective core potentials is a reliable approach when dealing with the chemical properties of metal centers in oxide surfaces.[24] For the hydrogen and sulfur atoms (H_2, H_2S, HS, and S adsorbates), we included all their electrons in the calculations. The molecular orbitals were expanded using Gaussian-type orbitals (GTOs). The atomic orbitals of H and S were expressed in terms of a double-ζ quality basis set augmented with polarization functions.[21,24] The 5s, 5p, and 4d atomic orbitals of Mo were explicitly treated by a basis set of three s, three p, and four d primitive GTOs contracted to two s, one p, and two d (3s3p4d/2s1p2d).[25] Basis sets obtained through a (3s3p5d/2s1p2d) contraction scheme were used to describe the 4s, 4p, and 3d atomic orbitals of Ni and Co.[25a,26] Finally, the valence orbitals of O were treated using the basis set recommended by Stevens, Basch, and Krauss.[23] Previous experience indicates that these basis sets provide satisfactory results for adsorption geome-

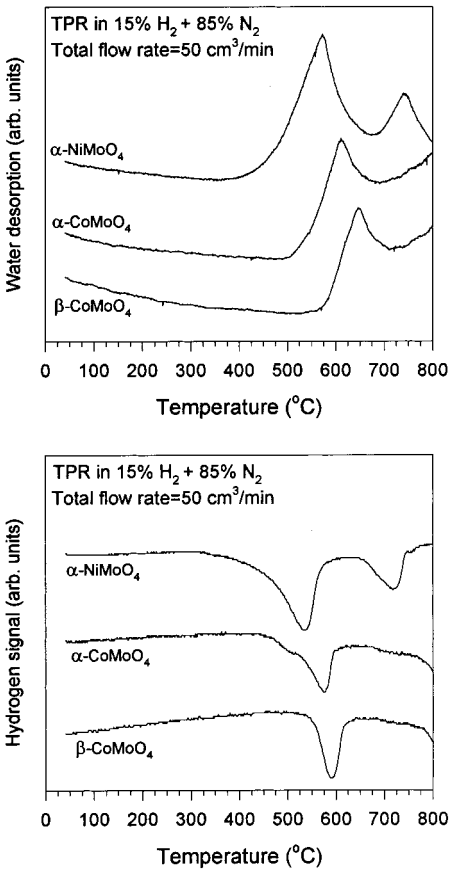

Figure 1. Hydrogen consumption (bottom part) and water desorption (top part) during the H_2-TPR of α-$NiMoO_4$, α-$CoMoO_4$, and β-$CoMoO_4$. Heating rate = 20 °C/min.

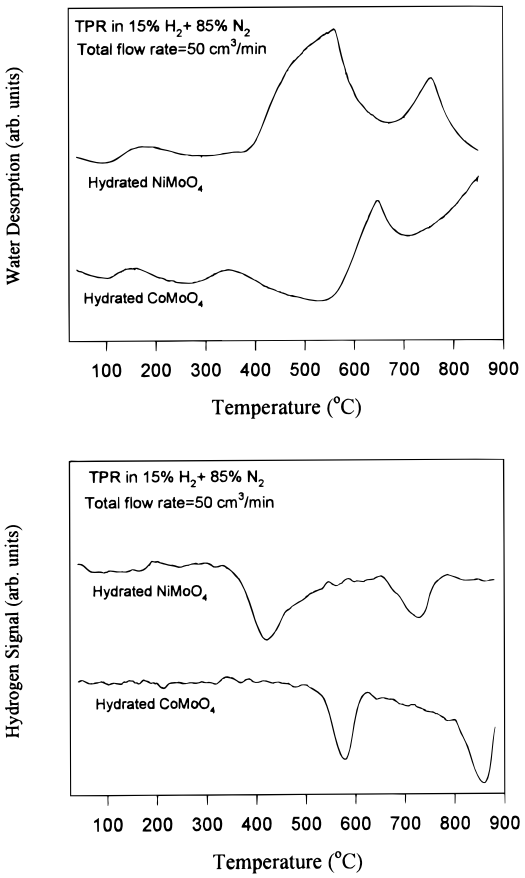

Figure 2. Hydrogen consumption (bottom part) and water desorption (top part) during the H_2-TPR of $NiMoO_4 \cdot nH_2O$ and $CoMoO_4 \cdot nH_2O$. Heating rate = 20 °C/min.

tries.[24−26] On the other hand, the energetics derived from these SCF calculations for adsorption reactions are not quantitative and simply provide a guide for the interpretation of experimental results.[24] The limited size of the basis sets and the lack of electron correlation introduce uncertainty in the computed bonding energies.[27,28] Despite this limitation, the use of ab initio SCF methods with cluster models has proved to be a very useful approach for studying a large variety of phenomena that occur on oxide surfaces.[24,27−29] This type of calculations become particularly powerful when combined with experimental studies[24] as done in the present article.

III. Results and Discussion

III.1. Reaction of H_2 with $CoMoO_4$ and $NiMoO_4$. Figure 1 shows spectra for the reduction of α-$NiMoO_4$, α-$CoMoO_4$, and β-$CoMoO_4$ in a gas mixture of H_2 and N_2. For α-$NiMoO_4$, the uptake of hydrogen begins around 400 °C and two peaks for desorption of water (α-$NiMoO_4$ + $H_{2,gas}$ → H_2O_{gas} + $NiMoO_x$) are seen at ∼ 550 and 730 °C. In the case of β-$NiMoO_4$ (not shown), the uptake of hydrogen starts above 500 °C with major consumption peaks at 605 and 690 °C.[10] For the cobalt molybdates, the reaction with hydrogen begins between 500 (α-$CoMoO_4$) and 550 °C (β-$CoMoO_4$) and the first water desorption peaks appear at 610−640 °C. When these data are compared with H_2-TPR data for pure molybdenum oxides,[30] one finds that the nickel and cobalt molybdates are more reactive toward H_2 than MoO_3 or MoO_2, compounds that show substantial interactions with hydrogen at temperatures well above 650 °C.

The TPR spectra for $NiMoO_4 \cdot nH_2O$ and $CoMoO_4 \cdot nH_2O$ are shown in Figure 2. The data for the consumption of hydrogen agree well with results of previous H_2-TPR studies.[10] The water desorption spectrum for the $CoMoO_4 \cdot nH_2O$ sample shows weak features between 100 and 400 °C as a result of the $CoMoO_4 \cdot nH_2O$ → β-$CoMoO_4$ + nH_2O_{gas} transformation,[15] and strong peaks above 550 °C as a consequence of the β-$CoMoO_4$ + $H_{2,gas}$ → nH_2O_{gas} + $CoMoO_x$ reaction. The water desorption spectrum for $NiMoO_4 \cdot nH_2O$ exhibits a small peak at 170 °C and intense features from 400 to 800 °C. The small peak can be attributed to the desorption of chemisorbed water from $NiMoO_4 \cdot nH_2O$,[15] whereas the strong features are a product of the reduction of this hydrate. In this case, reaction with H_2 starts before the temperature necessary for a complete $NiMoO_4 \cdot nH_2O$ → β-$NiMoO_4$ + nH_2O_{gas} transformation,[15] and one sees a water desorption spectrum very different from those observed during the reduction of β-$NiMoO_4$ and α-$NiMoO_4$.

The TPR results in Figures 1 and 2 indicate that, in general, the nickel molybdates are more reactive toward H_2 than the cobalt molybdates. This is corroborated by the X-ray powder diffraction data in Figure 3. The figure displays diffraction patters for β-$NiMoO_4$, α-$NiMoO_4$, β-$CoMoO_4$, and reduced samples of the molybdates (R:α-$NiMoO_4$ and R:β-$CoMoO_4$). Not shown are the diffraction patterns of the reduced $NiMoO_4 \cdot nH_2O$ and $CoMoO_4 \cdot nH_2O$ compounds which were very similar to those displayed for R:α-$NiMoO_4$ and R:β-$CoMoO_4$, respectively. In these experiments, the pure molybdates were put in a reaction cell under a 15%H_2/85%N_2 mixture (flow rate = 50 cm^3/min) and the temperature was ramped from 25 to 600 °C (20 °C/min). After that, the reduced samples were cooled to room temperature, exposed to oxygen from the atmosphere, and the XRD patterns were taken. In subsequent TPR experiments with the samples exposed to the atmosphere, we found that the

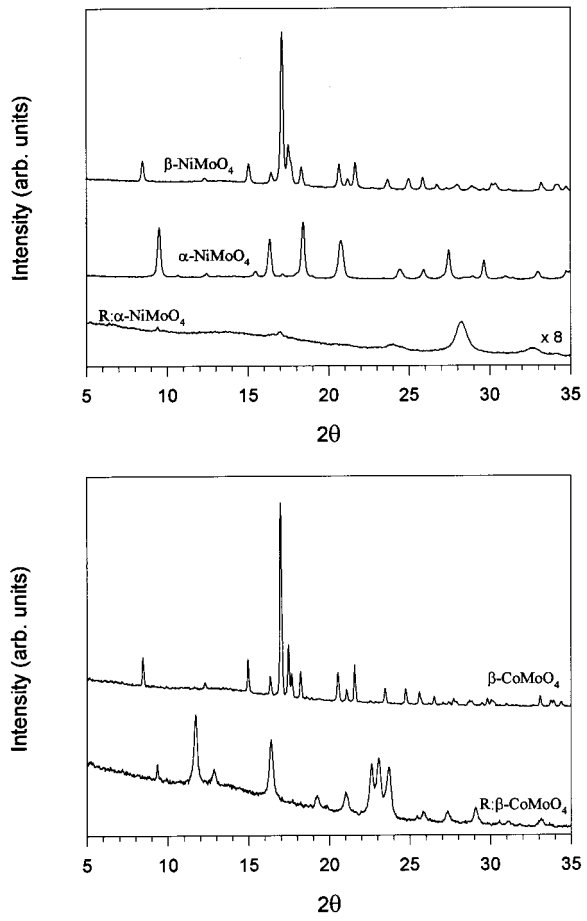

Figure 3. X-ray powder diffraction patterns for pure and reduced nickel molybdates (top part), plus pure and reduced β-$CoMoO_4$ (bottom part). To prepare the reduced samples, α-$NiMoO_4$ and β-$CoMoO_4$ were put in a reaction cell under a H_2/N_2 mixture and the temperature was ramped from 25 to 600 °C. Then, the partially reduced oxides were cooled to room temperature, exposed to atmospheric oxygen, and finally the powder diffraction patterns were taken. A wavelength of 1.004 Å was used to take these XRD data.

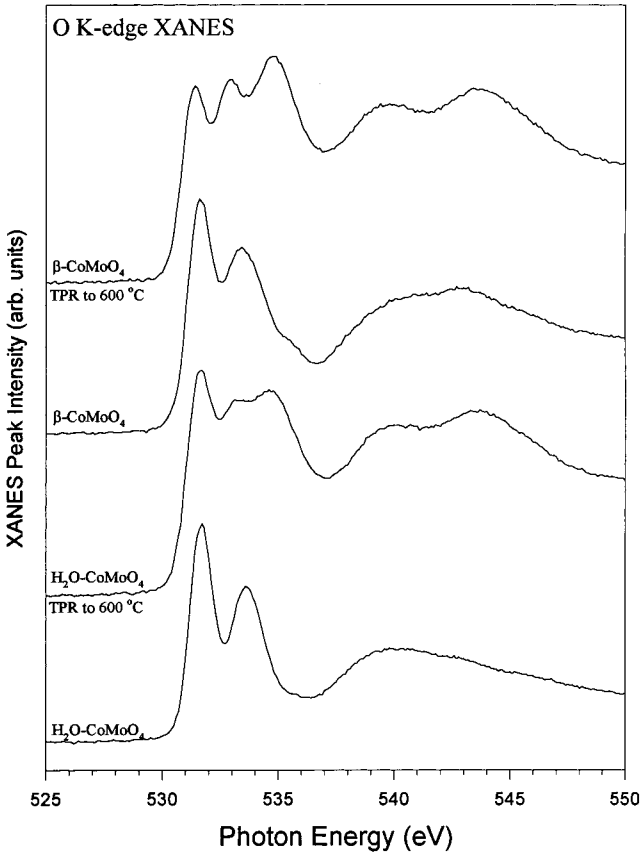

Figure 4. O K-edge XANES spectra for pure and reduced β-$CoMoO_4$ and $CoMoO_4 \cdot nH_2O$. All the spectra were recorded at room temperature. To prepare the reduced samples, β-$CoMoO_4$ and $CoMoO_4 \cdot nH_2O$ were put in a reaction cell under a $15\%H_2/85\%N_2$ mixture (flow rate = 50 cm^3/min) and the temperature was ramped from 25 to 600 °C (20 °C/min). Then the partially reduced oxides were cooled to room temperature, exposed to atmospheric oxygen, and the XANES spectra taken.

reduced cobalt molybdates did not react with H_2 at temperatures between 25 and 600 °C (i.e., they did not adsorb significant amounts of oxygen when exposed to the atmosphere after the initial reduction with H_2). In the case of the reduced nickel molybdates, subsequent TPR showed consumption of small amounts of H_2 between 400 and 500 °C, indicating that these samples adsorbed some oxygen when exposed to the atmosphere after the reduction treatment. The procedure followed here for the reduction of the cobalt and nickel molybdates is similar to that used in previous works[11,30] where these bimetallic oxides were partially reduced to enhance their catalytic activity.

The reduced β-$CoMoO_4$ and $CoMoO_4 \cdot nH_2O$ samples had identical X-ray powder patterns at room temperature. These diffraction patterns were well defined (see bottom part of Figure 3) and by comparison to XRD data reported in the literature[31] can be assigned to a mixture of $Co_2Mo_3O_8$ (major component) and another oxide (diffraction lines at 19.3, 22.5, and 27.4°; d = 2.99, 2.57, and 2.11 in agreement with calculations by Haber and Janas for Co_2MoO_4[31b]). The powder diffraction patterns for the reduced α-$NiMoO_4$ and $NiMoO_4 \cdot nH_2O$ samples were very weak and ill defined. A broad peak centered at 28.2° was observed (see top part in Figure 3), which together with the much less intense signal at around 32.5° can be attributed to Ni[32a] and/or Ni_4Mo.[32b] Feeble signals at ca. 17 and 24° can be assigned to amorphous MoO_2.[32c] (It must be noted that, after the reduction treatment, some O_2 reacted with this sample, and the main XRD peak of NiO[32d] at 27.8° is close to the broad signal observed at 28.2°). Thus, for the nickel molybdates the degree of reduction was more extensive than for the cobalt molybdates producing amorphous systems that probably contained metallic nickel and a molybdenum oxide.

It is well-known that the O K-edge XANES features can be used to distinguish oxygen atoms under different bonding environments in oxides.[33−35] The case of the cobalt and nickel molybdates is particularly interesting because these oxides contain two different metals. In principle, one can have electron transfer from the O 1s orbitals into the empty orbitals of both metals. Nevertheless, the O 1s electrons are mainly excited into the Mo(4d,5s,5p) orbitals.[15] For $CoMoO_4$ and $NiMoO_4$, the features near the threshold in the O K-edge spectra track very well the splitting of the Mo 4d orbitals in tetrahedral and octahedral fields and can be very useful for probing the local symmetry of Mo atoms in molybdenum oxides.[15] Figure 4 shows O K-edge XANES spectra for pure and reduced cobalt molybdates. In β-$CoMoO_4$ and $CoMoO_4 \cdot nH_2O$, Mo^{6+} is in a tetrahedral environment[14,15] and its empty 4d orbitals split into e and t levels that lead to the two peaks near the O 1s edge as a result of O 1s → Mo 4d(e) and O 1s → Mo 4d(t) electronic transitions. After reducing these oxides, one obtains a mixture of $Co_2Mo_3O_8$ and a second oxide, probably Co_2MoO_4 (see above). Clear changes are seen in the O K-edge spectra. Now, between 530 and 535 eV there are at least three overlapping features and broad peaks appear at 540 and 545 eV. In $Co_2Mo_3O_8$, the average oxidation state of the Mo atoms is lower

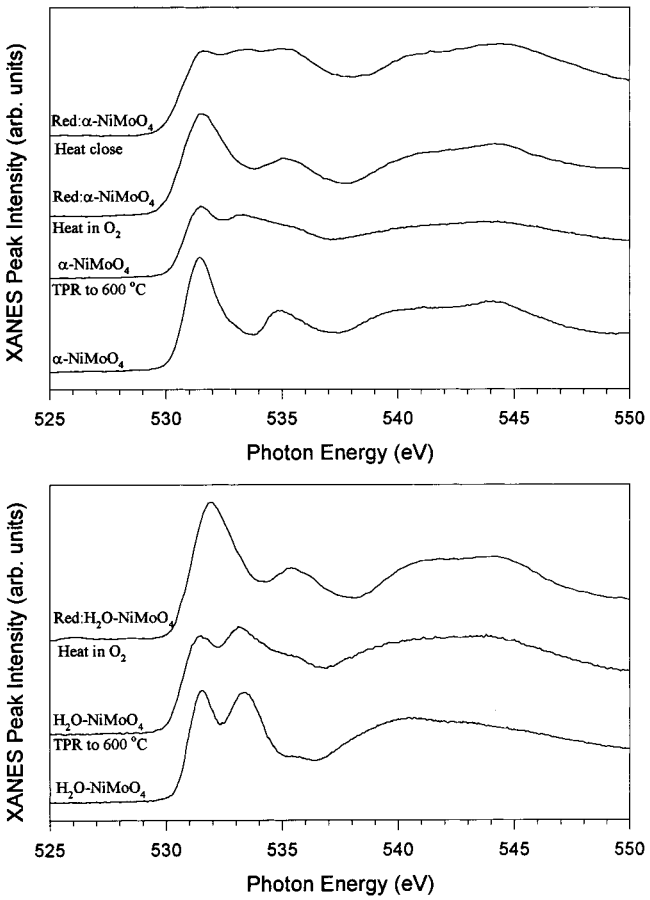

Figure 5. Top part: O K-edge XANES spectra for pure, reduced, and reoxidized α-$NiMoO_4$. Bottom part: Similar data for $NiMoO_4 \cdot nH_2O$. The nickel molybdates were reduced following the procedure described in Figure 4. XANES spectra were taken, and then the reduced samples (R:α-$NiMoO_4$ and R:$H_2O-NiMoO_4$) were heated in air or in a closed capillary from 25 to 650 °C. In the final step, the samples were cooled to room temperature and XANES spectra were recorded.

than 6+, electrons occupy the Mo 4d shell, and more than two types of O 1s → Mo 4d transitions are possible in octahedral and tetrahedral environments.[36] Thus, for reduced β-$CoMoO_4$ and $CoMoO_4 \cdot nH_2O$, the multiple features between 530 and 535 eV in the O K-edge can be attributed to O 1s → Mo 4d transitions. One of these features (at ∼ 533 eV) and the peaks at 540 and 544 eV match well peaks seen in the O K-edge spectra of "CoO" type compounds.[37] In β-$CoMoO_4$ and $CoMoO_4 \cdot nH_2O$, the empty orbitals of Mo^{6+} are probably much more stable (i.e., appear at lower energy) than the empty orbitals of Co^{2+}, favoring O 1s → Mo(4d,5s,5p) transitions over O 1s → Co(3d,4s,4p) transitions. Once the oxidation state of Mo is reduced, the stability of the empty orbitals of Mo decreases due to electron−electron repulsion, and the O 1s → Co(3d,4s,4p) transitions can compete with the O 1s → Mo(4d,5s,5p) transitions. It is likely that this competition produces the rich O 1s spectra seen for the reduced β-$CoMoO_4$ and $CoMoO_4 \cdot nH_2O$ samples.

Figure 5 displays O K-edge spectra for pure and reduced nickel molybdates. In α-$NiMoO_4$, the Mo atoms are in an octahedral environment,[15] and two peaks are observed between 530 and 535 eV with a separation of ∼ 3.5 eV. For $NiMoO_4 \cdot nH_2O$, the Mo atoms are in a tetrahedral environment,[15] and two peaks are also observed between 530 and 535 eV, but they are separated by only 1.8 eV. This difference, which reflects variations in the splitting of the Mo 4d orbitals in octahedral and tetrahedral fields,[15] practically disappears once the nickel molybdates are reduced. The reduced nickel molybdates exhibit multiple overlapping features from 530 to 535 eV that can be attributed to O 1s → Mo 4d transitions in systems in which the Mo atoms have oxidation states substantially lower than 6+.[36] These features are not as well defined as those observed in the O K-edge spectra of the reduced cobalt molybdates (see Figure 4), reflecting the amorphous nature of the reduced $NiMoO_4$ samples.

We were able to obtain the Mo M_{III}-edge XANES spectra of the reduced nickel molybdates (this was not possible for the reduced cobalt molybdates due to overlap of Co and Mo features). These spectra did not show the two well-defined peaks (Mo 3p → Mo 4d(t) and Mo 3p → Mo 4d(e) electronic transitions) characteristic of the $NiMoO_4$ and $NiMoO_4 \cdot nH_2O$ compounds.[15,33] Instead, they showed a single and broad peak, with the peak maximum at energies of 397.8−398.0 eV. These energies are much closer to that that seen for the peak maximum of MoO_2 (397.6 eV) than to those observed for the peak maxima of MoO_3 (398.5 eV) or the pure nickel molybdates (398.5−398.6 eV). Such a behavior indicates a substantial reduction in the average oxidation state of Mo (6+ → 4+).[33] For the reduction of $NiMoO_4$ compounds, it has been previously proposed that the first H_2-consumption feature in TPR (below 600 °C, see Figure 1) leads to the formation of Ni or Ni_4Mo intermetallics dispersed in amorphous MoO_2.[10,32e] Our XANES and XRD results are consistent with this picture.

The experimental data described above show important differences in the reactivities of $NiMoO_4$, $CoMoO_4$, and pure molybdenum oxides toward H_2. We investigated the adsorption and dissociation of H_2 on these oxides at a molecular orbital level. Figure 6 displays the type of cluster that was used to model the interaction of H_2 with surfaces of α-$NiMoO_4$, α-$CoMoO_4$, and α-MoO_3 in our ab initio SCF calculations. The objective here is to compare the behavior of Mo, Co, and Ni atoms that have an identical number of oxygen neighbors. We are interested in differences in the intrinsic reactivity of these metal atoms. The clusters in Figure 6 represent a cut in the crystal structure of α-$NiMoO_4$,[14] α-$CoMoO_4$,[14a] and α-MoO_3,[38] that produces a plane in which each metal center is missing only one oxygen neighbor. Such a plane is supposed to be stable and chemically active in this kind of oxides.[7] This is the (010) face of α-MoO_3.[38b] In our model clusters, the ratio of metal-to-oxygen atoms ($Ni_3Mo_3O_{13}^{2-}$, $Co_3Mo_3O_{13}^{2-}$, and $Mo_4O_{13}^{2-}$) was close to the stoichiometry of $NiMoO_4$, $CoMoO_4$, and MoO_3. The metal and oxygen atoms were set at geometries derived from XRD studies for the bulk oxides.[14,38] The clusters also contained a large set of positive and negative point charges (cNi = +2e, cCo = +2e, cMo = +6e, cO = −2e) arranged in three layers: $Ni_3Mo_3O_{13}/cNi_9cMo_9cO_{35}$, $Co_3Mo_3O_{13}/cCo_9cMo_9cO_{35}$, and $Mo_4O_{13}/cMo_{16}cO_{47}$. Previous studies show that this approach mimics the effects of the Madelung field in oxide surfaces.[24c,28,29,39]

In Table 1 are listed the calculated bonding energies and bond distances for the adsorption of a hydrogen atom on metal (M_1 = Ni, Co, or Mo) and O_1 sites of the model clusters. The M_1 atoms are pentacoordinated, whereas the O_1 atoms are only dicoordinated. The ASED-MO method has been used to study the interaction of H with a $Mo_6O_{25}^{14-}$ cluster, and a value of 31 kcal/mol has been predicted for the adsorption energy on a dicoordinated O atom, with the adsorption energy on pentacoordinated Mo atoms varying from 29 to 58 kcal/mol.[40] In Table 1, the metal ↔ H interactions are considerably stronger than the O ↔ H interactions. Among the metals, nickel shows the strongest bonding interactions with H, while molybdenum

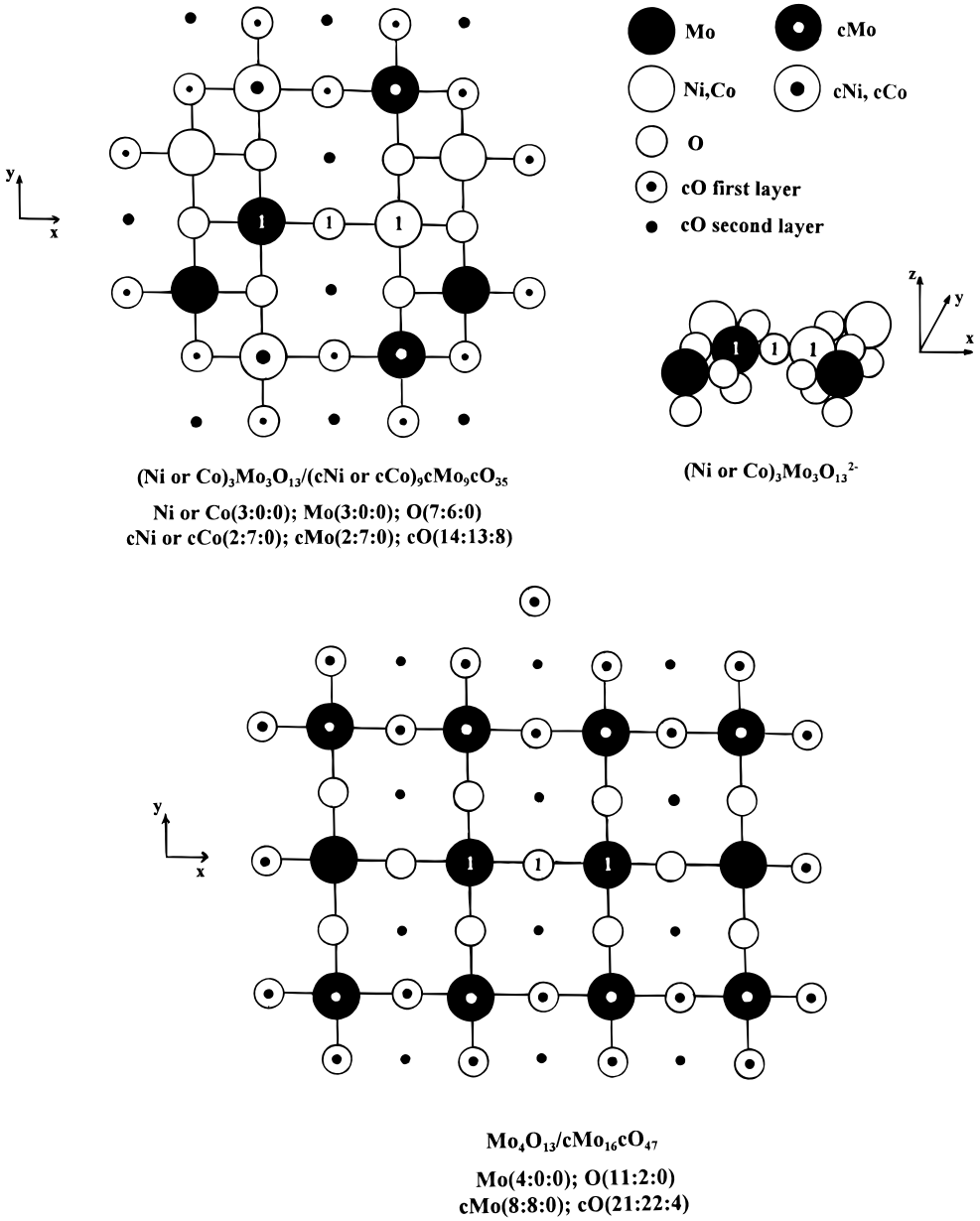

Figure 6. Clusters used to model the adsorption and dissociation of H_2 on surfaces of α-$NiMoO_4$ (top), α-$CoMoO_4$(top), and α-MoO_3 (bottom). The clusters contain metal and oxygen atoms plus positive and negative point charges arranged in three layers. The notation (a:b:c) specifies how many atoms or point charges are in each layer. Metal and oxygen atoms that represent adsorption sites (AS) are labeled "1". For the $Ni_3Mo_3O_{13}$/$cNi_9cMo_9cO_{35}$ and $Co_3Mo_3O_{13}$/$cCo_9cMo_9cO_{35}$ clusters, the first layer contains 7 oxygen and 6 metal atoms. In addition, there are 6 oxygen atoms in the second layer (directly below the first-layer metal atoms). In the case of the Mo_4O_{13}/$cMo_{16}cO_{47}$ cluster, the first layer contains 11 oxygen and 4 Mo atoms, with two oxygen atoms in the second layer underneath the Mo_1 atoms. In these clusters, the point charges were set at the positions expected for the metal and oxygen atoms in the bulk oxides.[14,38] In the figure, we show the position for the point charges present in the first layer of the clusters, plus some of the negative point charges in the second layer (·).

exhibits the weakest.[41] Identical trends were seen for the adsorption of a H_2 molecule (see Table 2). The molecule was oriented with its H−H axis either vertical or parallel to the surface (along the *z* or *y* axis in Figure 6, respectively). This produced one or two M_1−H bonds. The stability of these adsorption geometries was very similar. An H_2 adsorption geometry in which both atoms are simultaneously bonded to a metal site is a probable precursor for the dissociation of the molecule. In these "parallel" configurations, the adsorption of the molecule leads to a significant increase (0.06−0.11 Å, see Table 2) in the H−H bond length. The SCF calculations predict that the dissociation of H_2 is a very exothermic process on a metal site (homolitic cleavage of the H−H bond, two M_1−H bonds) or on a combination of metal and oxygen sites (heterolitic cleavage of the H−H bond, M_1−H, and M_1−O bonds). When comparing pentacoordinated metal sites and dicoordinated oxygen sites, H_2 dissociation should occur preferentially on metal sites. The results in Table 2 indicate that the reactivity of the oxides toward H_2 increases in the sequence: MoO_3 < $CoMoO_4$ < $NiMoO_4$. Interestingly, the Mo_1 and O_1 sites of the cobalt− and nickel−molybdate clusters are somewhat more reactive than similar sites in the MoO_3 cluster. This could be a consequence of Co(or Ni) ↔ O and Co(or Ni) ↔ O ↔ Mo electronic interactions that enhance the chemical activity of the Mo and O sites.

Since the presence of nickel has such a large effect on the energetics of H_2 dissociation, it is worthwhile to examine the interaction of H_2 with the $Ni_3Mo_3O_{13}$/$cNi_9cMo_9cO_{35}$ cluster in more detail. Figure 7 shows the energy profile associated with the dissociation of H_2 on a Ni_1 or Mo_1 site of the cluster. In the

TABLE 1: Adsorption of Atomic H on MoO_3, $CoMoO_4$, and $NiMoO_4$ Clusters

	bonding energy (kcal/mol)	AS−H (Å)[a]
H on MoO_3: $HMo_4O_{13}/cMo_{16}cO_{47}$		
on Mo_1	−58	1.72
on O_1	−42	1.07
H on $CoMoO_4$: $HCo_3Mo_3O_{13}/cCo_9cMo_9cO_{35}$		
on Mo_1	−60	1.69
on Co_1	−66	1.63
on O_1	−45	1.06
H on $NiMoO_4$: $HNi_3Mo_3O_{13}/cNi_9cMo_9cO_{35}$		
on Mo_1	−61	1.69
on Ni_1	−74	1.62
on O_1	−46	1.03

[a] AS (adsorption site) = Mo_1, Co_1, Ni_1, or O_1.

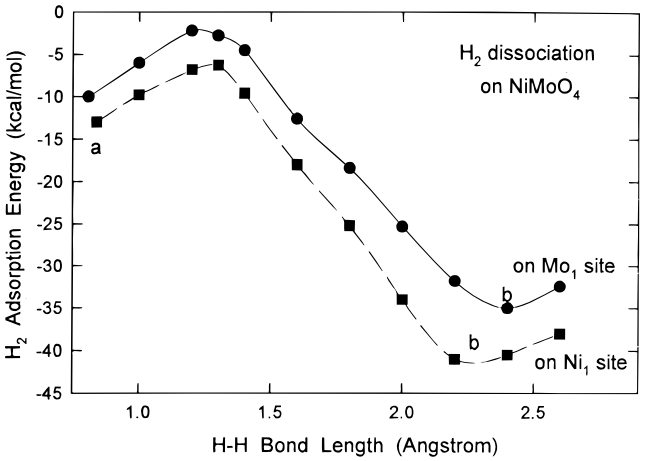

Figure 7. Dissociation of H_2 on Mo_1 or Ni_1 sites of the $Ni_3Mo_3O_{13}/cNi_9cMo_9cO_{35}$ cluster. H_2 was adsorbed on the adsorption site with its molecular axis parallel to the surface and the hydrogens pointing along the *y* axis in Figure 6. The H−H bond was elongated, and the two similar Mo_1−H or Ni_1−H distances were optimized. The initial configurations (point a, H_2 molecule) were H−H = 0.81 Å, Mo_1−H = 1.81, and 1.81 Å on the Mo_1 site; and H−H = 0.84 Å, Ni_1−H = 1.74 and 1.74 Å on the Ni_1 site. At the minima (point b, 2H atoms), the configurations were H−H = 2.40 Å, Mo_1−H = 1.72 and 1.73 Å on the Mo_1 site, and H−H = 2.20 Å, Ni_1−H = 1.65 and 1.64 Å on the Ni_1 site. The adsorption energy was calculated using the isolated $Ni_3Mo_3O_{13}/cNi_9cMo_9cO_{35}$ cluster and the free H_2 molecule as reference state.

"initial state" for these systems, H_2 was in the optimized structure for molecular adsorption (see Table 2). H_2 was adsorbed with its molecular axis parallel to the surface (two similar Ni_1−H or Mo_1−H bonds) and the hydrogens pointing along the *y* axis in Figure 6. The results in Figure 7 indicate that there is an energy barrier for the dissociation of H_2. On the Mo_1 site, the size of the barrier is ∼8 kcal/mol, and in the "transition state" (i.e., top of the barrier) the molecule is weakly bound to the surface, favoring desorption instead of dissociation of H_2. On Ni_1, there is a small reduction in the size of the energy barrier and a substantial enhancement in the adsorption energy of the "transition state". These effects, together with an increase in the stability of the final products, make much easier the dissociation of the H_2 molecule on Ni sites.[41]

During the H_2-TPR of $CoMoO_4$, $NiMoO_4$, and MoO_3, water is formed as a product. We found that the reaction:

$$H_2(gas) + Cluster \rightarrow \{Cluster - O_1\} + H_2O(gas) \quad (1)$$

is more difficult (i.e., 6−8 kcal/mol less exothermic[42]) on the MoO_3 cluster than on the $CoMoO_4$ and $NiMoO_4$ clusters. In these systems, the removal of the dicoordinated O_1 atom requires much less energy than the removal of O atoms that are tri and tetracoordinated.[43] In general, the SCF calculations predict that in the clusters the Ni−O and Co−O bonds are weaker than the Mo−O bonds. This is consistent with trends seen for the dissociation energies of diatomic molecules (NiO ≈ CoO ≪ MoO)[44] and the heats of formation of bulk oxides (NiO ≈ CoO < MoO_2 < MoO_3).[45]

On the basis of the theoretical results, one can explain differences observed in the behavior of $NiMoO_4$, $CoMoO_4$, and MoO_3 during H_2-TPR experiments. In these experiments, the cobalt and nickel molybdates are reduced at temperatures

TABLE 2: Adsorption of H_2 Molecule on MoO_3, $CoMoO_4$, and $NiMoO_4$ Clusters

	bonding energy (kcal/mol)	H−H (Å)	AS−H (Å)[a]
Free H_2		0.73	
H_2 on MoO_3: $H_2Mo_4O_{13}/cMo_{16}cO_{47}$			
on Mo_1, vertical	−7	0.77	1.76
on Mo_1, parallel	−8	0.79	1.79, 1.79
on Mo_1 and Mo_1 (2H)	−32		1.73, 1.73
on Mo_1 and O_1 (2H)	−23		1.69(1.06)[b]
H_2 on $CoMoO_4$: $H_2Co_3Mo_3O_{13}/cCo_9cMo_9cO_{35}$			
on Mo_1, vertical	−7	0.76	1.78
on Mo_1, parallel	−6	0.79	1.81, 1.81
on Mo_1 and Mo_1 (2H)	−34		1.72, 1.71
on Mo_1 and O_1 (2H)	−26		1.71(1.05)[b]
on Co_1, vertical	−9	0.78	1.69
on Co_1, parallel	−10	0.83	1.76, 1.76
on Co_1 and Co_1 (2H)	−37		1.65, 1.63
on Co_1 and O_1 (2H)	−29		1.62(1.06)[b]
H_2 on $NiMoO_4$: $H_2Ni_3Mo_3O_{13}/cNi_9cMo_9cO_{35}$			
on Mo_1, vertical	−8	0.77	1.77
on Mo_1, parallel	−10	0.81	1.81, 1.81
on Mo_1 and Mo_1 (2H)	−35		1.72, 1.73
on Mo_1 and O_1 (2H)	−25		1.70(1.04)[b]
on Ni_1, vertical	−10	0.80	1.68
on Ni_1, parallel	−13	0.84	1.74, 1.74
on Ni_1 and Ni_1 (2H)	−41		1.65, 1.64
on Ni_1 and O_1 (2H)	−32		1.63(1.03)[b]

[a] AS (adsorption site) = Mo_1, Co_1, or Ni_1. [b] O_1−H bond distance.

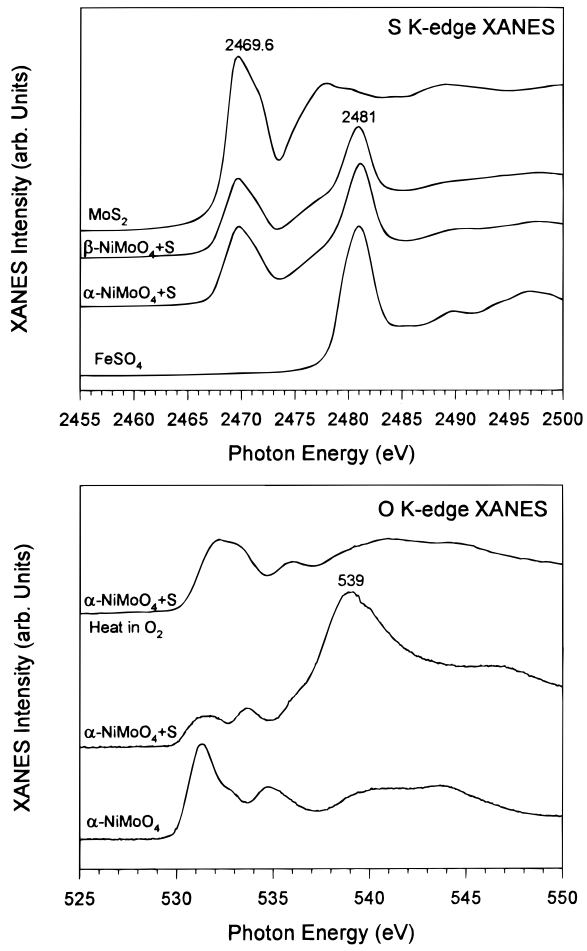

Figure 8. Top part: S K-edge XANES spectra of MoS_2, α-$NiMoO_4$-(sulfided), β-$NiMoO_4$ (sulfided) and $FeSO_4$. Bottom part: O K-edge spectra for α-$NiMoO_4$, α-$NiMoO_4$(sulfided), and the sulfided sample exposed to oxygen from the air at temperatures between 25 and 650 °C.

substantially lower (100−150 °C) than those reported for the reduction of pure molybdenum oxides (MoO_2, MoO_3).[30] The mixed-metal oxides are easier to reduce due to a combination of two fundamental properties. First, it is easier to adsorb and dissociate H_2 on Ni or Co sites than on Mo sites of an oxide. And second, as a result of differences in the strength of the metal−oxygen bonds, it is easier to remove oxygen as water from the nickel and cobalt molybdates than from MoO_3 or MoO_2. The fact that the $NiMoO_4$ compounds are more reactive toward H_2 than the $CoMoO_4$ compounds reflects differences in the intrinsic chemical activity of the Ni and Co sites.[46]

III.2. Reaction of H_2S with $NiMoO_4$ and $CoMoO_4$. In this section we examine the adsorption and dissociation of H_2S on nickel and cobalt molybdates. Two reasons motivate our interest in this chemical reaction. Currently, due to the negative effects of sulfur poisoning,[24c,47] there is a general desire to understand how sulfur-containing molecules interact with oxide surfaces. In addition, it has been shown that sulfided $NiMoO_4$ and $CoMoO_4$ compounds are very good precursors for hydrodesulfurization (HDS) catalysts.[9,10]

The top part in Figure 8 shows S K-edge XANES spectra acquired after exposing α- and β-$NiMoO_4$ to H_2S at 400 °C. Also shown for reference are the corresponding spectra for MoS_2 and a salt that contains a sulfate ($FeSO_4$). The S K-edge spectrum of MoS_2 is characterized by an intense edge at 2469.6 eV followed by additional features at −2478 and 2488 eV. Similar features are seen in the spectrum reported for NiS.[48]

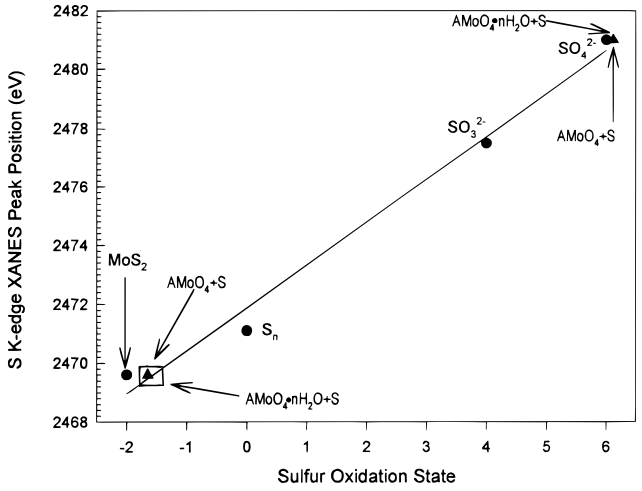

Figure 9. Plot of the sulfur oxidation state versus the S K-edge XANES peak position. The values for the reference compounds (MoS_2, S_n, Na_2SO_3, and Na_2SO_4) are denoted by filled circles and the data is fitted to a straight line ($r = 0.99$). The values for the sulfided $AMoO_4$ and $AMoO_4 \cdot nH_2O$ samples (A = Co or Ni) are indicated by triangles and set on the line. All the sulfided molybdates contain at least two different kinds of sulfur species in two distinct oxidation states (−1.7 and +6).

The S K-edge for $FeSO_4$ occurs nearly 11 eV higher than the one for MoS_2 or NiS. The sulfided α- and β-$NiMoO_4$ samples show clear peaks around 2469.5 and 2481 eV. An identical result was obtained after dosing H_2S to the $NiMoO_4 \cdot nH_2O$, β-$CoMoO_4$, and $CoMoO_4 \cdot nH_2O$ samples. This suggests the presence of at least two kinds of sulfur species in the sulfided molybdates. Several earlier studies have demonstrated that the position of the S K-edge XANES spectra can be used to characterize the oxidation state of sulfur.[35,49] Figure 9 shows a plot of the sulfur oxidation state versus the XANES peak position. The filled circles for MoS_2, S_n, SO_3^{2-}, and SO_4^{2-} come from reference compounds and correspond to sulfur oxidation states of −2, 0, +4, and +6 (respectively). The data were fitted (solid line) with a least-squares line ($r = 0.99$). The energy positions of the two peaks seen in the sulfided $AMoO_4$ and $AMoO_4 \cdot nH_2O$ compounds (A = Co or Ni) are indicated by triangles in the regression line. It can be clearly seen that there are at least two sulfur species present in each of the sulfided molybdates. The sulfur appearing at a photon energy of ∼ 2469.5 eV (average oxidation state ∼1.7, the box around these data point indicates the range of values observed) is associated with the presence of metal−sulfur bonds (MoS_x, NiS_x, or CoS_x). On the other hand, the XANES feature appearing at 2481 eV (oxidation state ∼ +6) can be attributed to the presence of sulfate species (SO_4^{2-}) that are formed by the reaction of sulfur with the oxygens of the molybdates.

Further proof for the formation of sulfate-type species was found in the O K-edge spectra of the sulfided samples. This is illustrated by the data in the bottom part of Figure 8 for an α-$NiMoO_4$ sample exposed to H_2S. After reaction with H_2S, the line shape of the O K-edge changes drastically. The small peaks between 530 and 535 eV are characteristic of metal oxides (see above), and the dominant feature at 539 eV denotes the presence of SO_4^{2-} in the sample.[50] The corresponding Ni K-edge XANES/EXAFS spectrum showed that at this point the system under study was very complex containing a mixture of $NiMoO_4$, $NiMoS_x$, and a sulfate.[50] We were able to obtain the Mo M_{III}-edge XANES spectra of the sulfided nickel molybdates (as for the case of the reduced samples, this was not possible for the sulfided cobalt molybdates due to the overlap of Co and Mo features). These spectra showed a single peak, as seen for

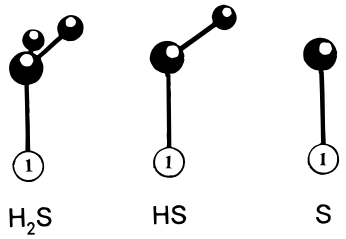

Figure 10. Adsorption geometries for H_2S, HS, and S on Mo_1 and Ni_1 sites of the $Ni_3Mo_3O_{13}/cNi_9cMo_9cO_{35}$ and $Mo_4O_{13}/cMo_{16}cO_{47}$ clusters.

MoS_2,[50] and not the two well-defined peaks typical of the pure nickel molybdates.[15,50] The peak maxima in the sulfided compounds (α-$NiMoO_4$ = 398.2 eV, β-$NiMoO_4$ = 397.9 eV, $NiMoO_4 \cdot nH_2O$ = 397.7 eV) appeared at energies between those observed for MoS_2 (397.0 eV)[50] and the pure nickel molybdates (398.5−398.6 eV). This is consistent with the fact that the mixed-metal oxides were only partially sulfided, and the trend in the peak positions suggests that the degree of sulfidation depends on the type of isomorph: $\alpha < \beta <$ hydrate. An identical sequence is observed for the catalytic activity of these compounds in HDS processes.[9,10] It can be argued that the sulfided $NiMoO_4 \cdot nH_2O$ would be a better HDS catalyst than the sulfided α and β isomorphs because it has a larger number of active $NiMoS_x$ sites. Previously, we have used a similar argument to explain differences in the HDS activity of sulfided α-$NiMoO_4$ and β-$NiMoO_4$.[50]

When comparing our results for the sulfidation of the cobalt and nickel molybdates with those reported for the sulfidation of MoO_3 or MoO_2,[30,51] one finds that it is much easier to sulfide the mixed-metal oxides than the pure molybdenum oxides. This difference is particularly well documented in the case of the $NiMoO_4$ isomorphs,[9,10] which can be fully sulfided without any problem.[10] On this basis, we decided to examine the interaction of α-$NiMoO_4$ and α-MoO_3 with H_2S, HS, and S at a molecular orbital level. Surfaces of these oxides were modeled using the clusters displayed in Figure 6, and the H_2S, HS, and S species were adsorbed on top of the Mo_1 or Ni_1 sites with the bonding configurations shown in Figure 10. Previous works[24a,c,d,52] have shown that H_2S preferentially adsorbs and dissociates on the metal centers of oxides. Our theoretical results predict that the $H_2S \leftrightarrow O$ interactions are weak on surfaces of $NiMoO_4$ and MoO_3. Thus, the SO_4^{2-} present in the sulfided molybdates is probably formed by migration of sulfur atoms from the metal centers onto the O sites.

Table 3 lists the calculated bonding energies and structural parameters for the adsorption of H_2S, HS, and S on the $Ni_3Mo_3O_{13}/cNi_9cMo_9cO_{35}$ and $Mo_4O_{13}/cMo_{16}cO_{47}$ clusters. The SCF calculations predict that H_2S adsorbs with its molecular plane slightly tilted (17−21°) with respect to the surface normal. In the case of HS, the calculated tilting in the molecular axis was more substantial (metal−S−H bond angle = 128°−137°). The predicted Mo−S and Ni−S bond lengths are within the range of values observed for this type of bonds in inorganic compounds.[6,53] The calculations showed minor changes (<0.03 Å) in the S−H bond lengths of H_2S and HS upon adsorption. A comparison of the adsorption energies on the MoO_3 and $NiMoO_4$ clusters shows that H_2S, HS, and S interact stronger with the Ni cations. This is illustrated by the results in Figure 11 for the $Ni_3Mo_3O_{13}/cNi_9cMo_9cO_{35}$ cluster. The adsorption energies of HS and S are the most affected when going from Mo to Ni, showing increases of 3−4 kcal/mol. HS and S have very large electron affinities[54,55] and display a tendency to behave as electron acceptors when bonded to surfaces.[24c,d,56] In

TABLE 3: Adsorption of H_2S, HS, and S on MoO_3 and $NiMoO_4$ Clusters

	bonding energy (kcal/mol)	H−S (Å)	AS−S (Å)[a]
Free H_2S		1.33	
Free HS		1.33	
MoO_3, $Mo_4O_{13}/cMo_{16}cO_{47}$			
H_2S on Mo_1	−8	1.33	2.41
HS on Mo_1	−13	1.34	2.40
S on Mo_1	−25		2.36
$NiMoO_4$, $Ni_3Mo_3O_{13}/cNi_9cMo_9cO_{35}$			
H_2S on Mo_1	−9	1.34	2.41
H_2S on Ni_1	−10	1.34	2.32
HS on Mo_1	−14	1.34	2.40
HS on Ni_1	−18	1.35	2.30
S on Mo_1	−27		2.35
S on Ni_1	−30		2.27

[a] AS (adsorption site) = Mo_1 or Ni_1.

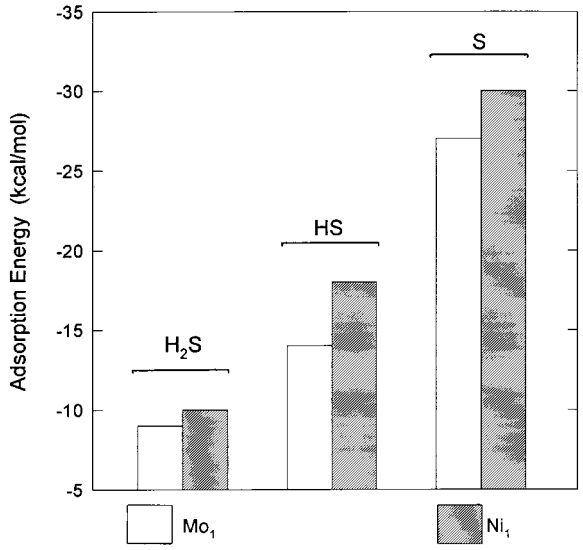

Figure 11. Adsorption energies calculated at the ab initio SCF level for H_2S, HS, and S on the $Ni_3Mo_3O_{13}/cNi_9cMo_9cO_{35}$ cluster. The S-containing species were adsorbed on the Mo and Ni atoms labeled "1" in Figure 6.

the $Ni_3Mo_3O_{13}/cNi_9cMo_9cO_{35}$ cluster, the oxidation state of the Ni atoms[57] was significantly lower (i.e., larger electron density) than that of the Mo atoms, favoring the formation of Ni → SH and Ni → S dative bonds. Since in general the adsorption bonds of HS and S are stronger than that of H_2S (see Table 3 and Figure 11), variations in the strength of the oxide−SH and oxide−S bonds probably determine the rate of decomposition of H_2S on the oxides. From this viewpoint, it is clear that $NiMoO_4$ should be easier to sulfide than MoO_3. In Table 3, the Mo_1 sites of the $NiMoO_4$ cluster are somewhat more active than similar sites in the MoO_3 cluster. An identical trend was observed for the adsorption of H (Table 1) and H_2 (Table 2). Ni ↔ O ↔ Mo electronic interactions probably enhance the chemical activity of the Mo sites in the $NiMoO_4$ system.

For the full sulfidation of MoO_3, a mechanism has been proposed that involves first reduction of the oxide by the hydrogens of H_2S ($MoO_3 \rightarrow MoO_2 \rightarrow Mo$), followed by sulfidation of the formed Mo metal ($Mo \rightarrow MoS_2$).[51] On the basis of this mechanism and the results presented in the previous section (i.e., easier to remove oxygen from $CoMoO_4$ and $NiMoO_4$ than from MoO_3), one can predict that the rate of sulfidation of the cobalt and nickel molybdates should be faster than that of MoO_3, as observed experimentally. The key here is the extra chemical reactivity that the Co and Ni atoms provide.

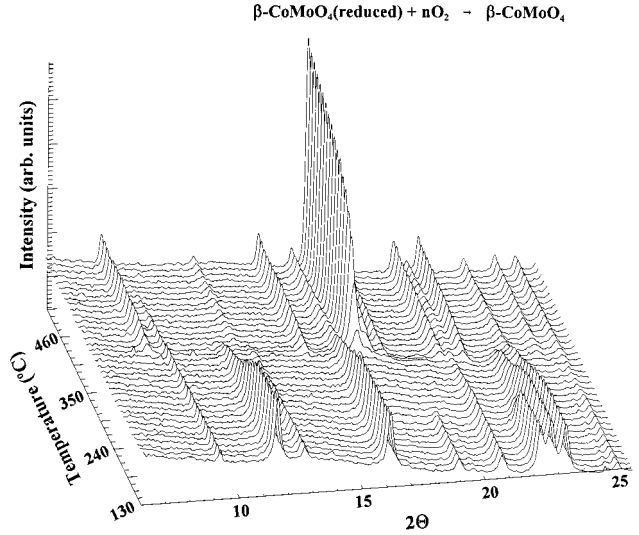

Figure 12. Time-resolved X-ray powder diffraction patterns for the oxidation of reduced β-$CoMoO_4$ in air. In the first step, the cobalt molybdate was reduced following the procedure described in section III.1. Then, the sample was set in an open capillary and heated from 25 to 650 °C ($\Delta T = 2.7$ °C/min). A wavelength of 1.004 Å was used to take these data.

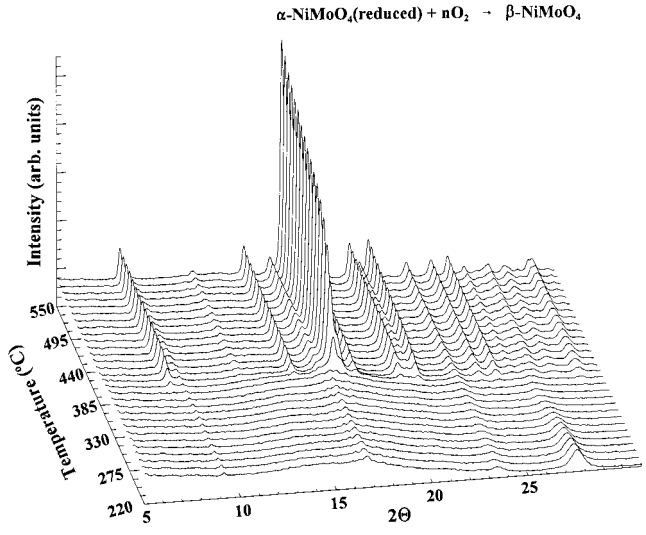

Figure 13. Time-resolved X-ray powder diffraction patterns for the oxidation of reduced α-$NiMoO_4$ in air. In the first step, the nickel molybdate was reduced following the procedure described in section III.1. Then, the sample was set in an open capillary and heated from 25 to 650 °C ($\Delta T = 2.7$ °C/min). A wavelength of 1.004 Å was used to take these data.

The behavior of the cobalt and nickel molybdates is a very good example of how one can enhance (i.e., promote) the chemical activity of an oxide by adding a second metal cation to the system.

III.3. Reoxidation of the Reduced and Sulfided Molybdates. When dealing with reduced and sulfided oxide catalysts, it is important to know how stable are they in oxygen and how difficult is it to regenerate the original oxides. In the case of sulfur poisoning, one can always attempt the removal of sulfur from the oxide by "burning" it in oxygen ($S_a + O_{2,gas} \rightarrow SO_{2,gas}$) at high temperature. Investigations at Brookhaven National Laboratory have recently established the feasibility of conducting subminute, time-resolved XRD experiments under a wide variety of temperature and pressure conditions (-190 °C $< T <$ 900 °C, $P \leq 45$ atm).[20] Using this unique approach we monitored the reoxidation of the reduced and sulfided molybdates as a function of temperature.

Figure 12 shows how the diffraction pattern of reduced β-$CoMoO_4$ changed when the sample was heated ($\Delta T = 2.7$ °C/min) in an open capillary that exposed it to oxygen from the air. Initially, the reduced β-$CoMoO_4$ contained a mixture of $Co_2Mo_3O_8$ (major component) and a second oxide. At temperatures between 25 and 180 °C, we did not see any changes in the powder pattern of the system. Around 180 °C, the second oxide present in the mixture started to transform into $Co_2Mo_3O_8$. From 210 to 270 °C, only diffraction lines for $Co_2Mo_3O_8$[31] were seen. Finally, around 300 °C β-$CoMoO_4$ appeared, became the dominant oxide in the diffraction pattern, and no additional changes were observed between 400 and 650 °C. After this treatment, the O K-edge XANES spectrum of the sample exhibited the typical features for β-$CoMoO_4$ showing that, indeed, there was a complete reoxidation of the system. We carried out experiments in which samples of reduced β-$CoMoO_4$ were heated in closed capillaries limiting the amount of oxygen present. In these cases, there was again a $Co_2Mo_3O_8 \rightarrow \beta$-$CoMoO_4$ transformation, but it occurred at 550−600 °C and did not produce a pure β-$CoMoO_4$ isomorph. Here, the final samples had a black color and O K-edge spectra that were more complex than that of β-$CoMoO_4$. The reduction of $CoMoO_4 \cdot nH_2O$ also produces a mixture of $Co_2Mo_3O_8$ and a second oxide (see above), and during the reoxidation of these samples we observed a behavior identical to that found for the reoxidation of reduced β-$CoMoO_4$.

Figure 13 displays time-resolved XRD data for the oxidation of reduced α-$NiMoO_4$ in the presence of air ($\Delta T = 2.7$ °C/min). For the nickel molybdates the reduction by reaction with H_2 was more extensive than for the cobalt molybdates, producing amorphous oxides and weak diffraction lines that can be attributed to a minor amount of poorly crystalline Ni, Ni_4Mo, and/or NiO (broad peak at 27−28°).[32] In the experiments of Figure 13, there was no change in the diffraction pattern of the sample at temperatures below 250 °C. Around 270 °C the main diffraction line at 27−28° began to disappear, but the peaks for β-$NiMoO_4$ did not appear until 370 °C. These peaks grew in intensity reaching a plateau at $\sim$ 500 °C. From this point and up to 650 °C, we did not see additional changes in the diffraction pattern of the sample. When the sample was allowed to cool to room temperature, it completely transformed into α-$NiMoO_4$ (as expected for pure β-$NiMoO_4$[15]) and exhibited the typical O K-edge XANES spectrum of this compound (see top part in Figure 5). During the heating of a sample of reduced α-$NiMoO_4$ from 25 to 650 °C with a limited amount of O_2 in the environment (closed capillary), we did not observe the formation of α- or β-$NiMoO_4$, and at the end the sample displayed an O K-edge spectrum very different from those of the pure $NiMoO_4$ isomorphs (see top part in Figure 5). The reoxidation of samples of reduced $NiMoO_4 \cdot H_2O$ led to the formation of β-$NiMoO_4$ at temperatures between 350 and 500 °C, which transformed into pure α-$NiMoO_4$ upon cooling to room temperature (see bottom part in Figure 5).

A comparison of the results in Figures 12 and 13 shows that it is easier to regenerate the $CoMoO_4$ oxides. The formation of β-$CoMoO_4$ starts at a substantially lower temperature ($\sim$70 °C) than the formation of β-$NiMoO_4$. This difference probably reflects the fact that initially the samples of the nickel molybdates were more reduced in the pretreatment with H_2 than the samples of the cobalt molybdates (see section III.1.). Also thermodynamic factors could play a role here, since β-$CoMoO_4$ is known to be more stable than β-$NiMoO_4$.[15] In general, our results showed no difficulties for regenerating pure $CoMoO_4$

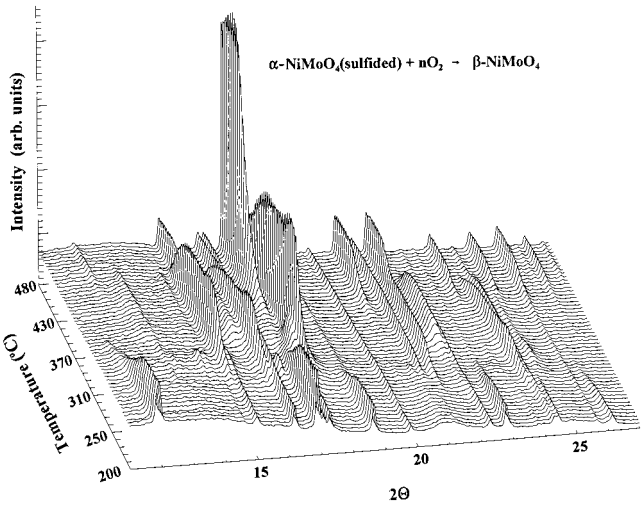

Figure 14. Time-resolved X-ray powder diffraction patterns for the oxidation of sulfided α-$NiMoO_4$ in air. In the first step, the nickel molybdate was sulfided following the procedure described in section II.2. Then the sample was set in an open capillary and heated from 25 to 650 °C (ΔT = 1.2 °C/min). A wavelength of 1.004 Å was used to take these data.

or $NiMoO_4$ when reduced samples of these oxides were exposed to O_2 at high temperatures. This was not the case when dealing with sulfided samples of the molybdates. "Burning" in O_2 was only partially successful for removing sulfur from the molybdates. A typical result is shown in Figure 14. After exposing α-$NiMoO_4$ to H_2S, one obtains a complex diffraction pattern that can be attributed to a mixture of α-$NiMoO_4$, MoS_2,[58] and $Ni_2Mo_3O_8$.[31a] This mixture is stable in air up to a temperature of 250 °C when clear changes occur in the X-ray powder pattern (see Figure 14). New diffraction lines appear, which probably originate in a compound of the $NiMoO_x$ type,[14,31,59] and the lines that could be assigned to MoS_2 disappear. Around 400 °C, the formation of β-$NiMoO_4$ starts, and only the diffraction pattern of this compound is observed at temperatures between 450 and 650 °C. After this treatment the sample showed a gray color, and upon cooling to room temperature we did not observe a complete β-$NiMoO_4$ → α-$NiMoO_4$ transformation. This suggest that some sulfur was still present in the sample. The corresponding O K-edge spectrum (bottom part in Figure 8) indicates that most of the sulfur (peak at 539 eV in the sulfided α-$NiMoO_4$, see section III.2.) was removed from the sample. In this spectrum, the line shape of the features from 530 to 535 eV is typical of a mixture of α- and β-$NiMoO_4$.[15]

IV. Summary and Conclusions

The reactivity of a series of cobalt and nickel molybdates (α-$AMoO_4$, β-$AMoO_4$, and $AMoO_4 \cdot nH_2O$, A = Co or Ni) toward H_2 was examined using temperature programmed reduction. In these experiments consumption of H_2 and formation of gaseous H_2O start at temperatures above 400 °C. In general, the cobalt and nickel molybdates are more reactive toward H_2 than MoO_2 or MoO_3: $MoO_2 < MoO_3 < CoMoO_4 < NiMoO_4$. After exposing the cobalt molybdates to H_2 at temperatures between 25 and 600 °C, the results of synchrotron-based XRD and XANES show a mixture that contains $Co_2Mo_3O_8$ (major component) and a second oxide (probably Co_2MoO_4). In the case of the nickel molybdates, a similar treatment produces very drastic changes leading to the formation of amorphous systems which may contain Ni, Ni_4Mo, and MoO_2. The interaction of H_2 with surfaces of α-$NiMoO_4$, α-$CoMoO_4$, and α-MoO_3 was investigated using ab initio SCF calculations. The mixed-metal oxides are easier to reduce due to a combination of two fundamental properties. First, it is easier to adsorb and dissociate H_2 on Ni or Co sites than on Mo sites of an oxide. And second, as a result of differences in the strength of the metal−oxygen bonds, it is easier to remove oxygen as water from the nickel and cobalt molybdates than from MoO_3 or MoO_2. The fact that the $NiMoO_4$ compounds are more reactive toward H_2 than the $CoMoO_4$ compounds reflects differences in the intrinsic chemical activity of the Ni and Co sites. The results of time-resolved XRD and XANES show that the reduced cobalt and nickel molybdates can be regenerated by reaction with O_2 at high temperature (350−450 °C). This treatment leads to the formation of the pure β-isomorph of these compounds.

After exposing the cobalt and nickel molybdates to H_2S at 400 °C, S K-edge XANES spectra show the presence of at least two types of sulfur species. One associated with a formal oxidation state of −2 (MoS_x, CoS_x, or NiS_x), and another associated with a formal oxidation state of +6 (SO_4^{2-}). The cobalt and nickel molybdates interact stronger with H_2S than MoO_3 or MoO_2. For the adsorption of H_2S, HS, and S on α-$NiMoO_4$ and α-MoO_3 clusters, the results of ab initio SCF calculations show bigger bonding energies on the Ni sites than on the Mo sites. In these systems, the oxidation state of the Ni atoms is substantially lower (i.e., larger electron density) than that of the Mo atoms, favoring the formation of Ni → SH and Ni → S dative bonds. From this viewpoint, it is clear that $NiMoO_4$ should be easier to sulfide than MoO_3. The results of time-resolved XRD and XANES show that most of the sulfur present in the sulfided $NiMoO_4$ and $CoMoO_4$ oxides can be removed by reaction with O_2 ($S_a + O_{2,gas} \rightarrow SO_{2,gas}$) at high temperatures (400−500 °C).

The key to the differences in the chemical reactivity of the MoO_3 and $AMoO_4$ (A = Co or Ni) compounds is in the properties of the cobalt and nickel atoms and the effects of Co ↔ O ↔ Mo and Ni ↔ O ↔ Mo interactions. The behavior of the cobalt and nickel molybdates is a very good example of how one can enhance the chemical activity of an oxide (MoO_3) by adding a second metal cation to the system.

Acknowledgment. The authors thank D.A. Fischer and F.-L. Lu for their help with the use of the U7A and X19A beam lines, respectively, at the NSLS. The NSLS is supported by the Divisions of Materials and Chemical Sciences of the U.S. Department of Energy. The work carried out at the Chemistry Department of BNL was supported under Contract DE-AC02-98CH10886 with the U.S. Department of Energy, Office of Basic Energy Sciences, Chemical Science Division. J.L.B. gratefully acknowledges a grant from ACS that made possible a visit to BNL.

References and Notes

(1) Kung, H. H. *Transition Metal Oxides: Surface Chemistry and Catalysis*; Elsevier: New York, 1989.

(2) (a) Satterfield, C. N. *Heterogeneous Catalysis in Industrial Practice, 2nd ed.*; McGraw-Hill: New York, 1991. (b) Ertl, G., Knözinger, H., Weitkamp, J., Eds. *Handbook of Heterogeneous Catalysis*; VCH: New York, 1997.

(3) Rodriguez, N. M., Soled, S. L., Hrbek, J., Eds. *Recent Advances in Catalytic Materials*; Fall Meeting of Materials, Research Society, Boston, December, 1997; Materials Research Society: Pittsburgh, 1998; Vol. 497.

(4) *Symposium on the Characterization of Mixed-Metal Oxide Catalysts*; 215th National Meeting of the American Chemical Society, Dallas, March, April, 1998; American Chemical Society: Washington, DC, 1998.

(5) Wyckoff, R. W. *Crystal Structures*, 2nd ed.; Wiley: New York, 1964.

(6) Wells, A. F. *Structural Inorganic Chemistry*, 6th ed; Oxford Press: New York, 1987.

(7) Henrich, V. A.; Cox, P. A. *The Surface Science of Metal Oxides*; University Press: Cambridge, 1994.

(8) Mazzocchia, C.; Aboumrad, C.; Diagne, C.; Tempesti, E.; Herrmann, J. M.; Thomas, G. *Catal. Lett.* **1991**, *10*, 181.

(9) Brito, J. L.; Barbosa, A. L.; Albornoz, A.; Severino, F.; Laine, J. *Catal. Lett.* **1994**, *26*, 329.

(10) Brito, J. L.; Barbosa, A. L. *J. Catal.* **1997**, *171*, 467 and references therein.

(11) Zou, J.; Schrader, G. L. *J. Catal.* **1996**, *161*, 667.

(12) Brito, J. L.; Laine, J. *Appl. Catal.* **1991**, *72*, L13.

(13) Madeley, R. A.; Wanke, S. *Appl. Catal.* **1988**, *39*, 295.

(14) (a) Smith, G. W.; Ibers, J. *Acta Crystallogr.* **1965**, *19*, 269. (b) Smith, G. W. *Acta Crystallogr.* **1962**, *15*, 1054. (c) Sleigth, A. W.; Chamberlain, B. L. *Inorg. Chem.* **1968**, *7*, 1672.

(15) Rodriguez, J. A.; Chaturvedi, S.; Hanson, J. C.; Albornoz, A.; Brito, J. L. *J. Phys. Chem. B* **1998**, *102*, 1347.

(16) Laine, J.; Pratt, K. C. *React. Kinet. Catal. Lett.* **1979**, *10*, 207.

(17) Mazzocchia, C.; Di Renzo, F.; Centola, P. *Rev. Port. Quim.* **1977**, *19*, 61.

(18) Fischer, D. A. Manuscript in preparation.

(19) Hastings, J. B.; Suortii, P.; Thomsolin, P.; Kvick, A.; Koetzle, T. *Nucl. Instrum. Methods* **1983**, *208*, 55.

(20) Norby, P.; Hanson, J. *Catal. Today* **1998**, *39*, 301 and references therein.

(21) Dupuis, M.; Chin, S.; Marquez, A. In *Relativistic and Electron Correlation Effects in Molecules and Clusters*; Malli, G. L., Ed.; NATO ASI Series 318; Plenum: New York, 1992.

(22) Hay, P. J.; Wadt, W. R. *J. Chem. Phys.* **1985**, *82*, 270.

(23) Stevens, W. J.; Basch, H.; Krauss, M. *J. Chem. Phys.* **1984**, *81*, 6026.

(24) (a) Rodriguez, J. A.; Chaturvedi, S.; Kuhn, M.; van Ek, J.; Diebold, U.; Robbert, P. S.; Geisler, H.; Ventrice, C. A. *J. Chem. Phys.* **1997**, *107*, 9146. (b) Rodriguez, J. A.; Chaturvedi, S.; Jirsak, T.; Hrbek, J. *J. Chem. Phys.* **1998**, *109*, 4052. (c) Rodriguez, J. A.; Chaturvedi, S.; Kuhn, M.; Hrbek, J. *J. Phys. Chem. B* **1998**, *102*, 5511. (d) Rodriguez, J. A.; Jirsak, T.; Chaturvedi, S.; Hrbek, J. *Surf. Sci.* **1998**, *407*, 171. (e) Chaturvedi, S.; Rodriguez, J. A.; Hrbek, J. *J. Phys. Chem. B* **1997**, *101*, 10860.

(25) (a) Rodriguez, J. A. *J. Phys. Chem. B* **1997**, *101*, 7524. (b) Rodriguez, J. A.; Kuhn, M. *Surf. Sci.* **1995**, *330*, L657.

(26) (a) Rodriguez, J. A. *Surf. Sci.* **1996**, *345*, 347. (b) Kuhn, M.; Rodriguez, J. A. *Surf. Sci.* **1996**, *355*, 85.

(27) (a) Whitten, J. L.; Yang, H. *Surf. Sci. Rep.* **1996**, *24*, 55. (b) van Santen, R. A.; Neurock, M. *Catal. Rev. Sci. Eng.* **1995**, *37*, 557.

(28) Ruette, F., Ed. *Quantum Chemistry Approaches to Chemisorption and Heterogeneous Catalysis*; Kluwer: Dordtrecht, 1992.

(29) Freund, H.-J.; Kulenbeck, H.; Staemmler, V. *Rep. Prog. Phys.* **1996**, *59*, 283.

(30) Brito, J. L.; Laine, J.; Pratt, K. C. *J. Mater. Sci.* **1989**, *24*, 425.

(31) (a) McCarroll, W. H.; Katz, L.; Ward, R. *J. Am. Chem. Soc.* **1957**, *79*, 5410. (b) Haber, J.; Janas, J. In *Reaction Kinetics in Heterogeneous Chemical Systems*; Barret, P., Ed.; Elsevier: Amsterdam, 1975; p 737.

(32) (a) JCPDS Powder Diffraction File No. 4-850. International Centre for Diffraction Data, Swarthmore, PA, 1989. (b) PDF No. 3-1036. (c) PDF No. 32-671. (d) PDF No. 44-1159. (e) Madeira, L. M.; Portela, M. F.; Mazzocchia, C.; Kaddouri, A.; Anouchinsky, R. *Catal. Today* **1998**, *40*, 229.

(33) Chen, J. G.; Fruhberger, B.; Colaianni, M. L. *J. Vac. Sci. Technol. A* **1996**, *14*, 1668.

(34) (a) Grunes, L. A.; Leapman, R. D.; Wilker, C. N.; Hoffmann, R.; Kunz, A. B. *Phys. Rev. B* **1982**, *25*, 7157. (b) de Groot, F. M. F.; Grioni, M.; Fuggle, J. C.; Ghijsen, J.; Sawatzky, G. A.; Petersen, H. *Phys. Rev. B* **1989**, *40*, 5715.

(35) Chen, J. G. *Surf. Sci. Rep.* **1997**, 30, 1.

(36) (a) Gray, H. B. *Electrons and Chemical Bonding*; Benjamin: New York, 1965; p 207. (b) Drago, R. S. *Physical Methods in Chemistry*; Saunders: New York, 1977; pp 379−390.

(37) de Groot, F. M. F.; Abbate, M.; van Elp, J.; Sawatzky, G. A.; Ma, Y. J.; Chen, C. T.; Sette, F. *J. Phys.* **1993**, *5*, 2277.

(38) (a) McCarron, E. M.; Thomas, D. M.; Calabrese, J. C. *Inorg. Chem.* **1987**, *26*, 370. (b) Firment, L. E.; Ferretti, A. *Surf. Sci.* **1983**, *129*, 155. (c) Michalak, A.; Hermann, K.; Witko, M. *Surf. Sci.* **1996**, *366*, 323.

(39) (a) Pacchioni, G.; Clotet, A.; Ricart, J. M. *Surf. Sci.* **1994**, *315*, 337. (b) Pacchioni, G.; Ferrari, A. M.; Bagus, P. *Surf. Sci.* **1996**, *350*, 159. (c) Lopez, N.; Illas, F. *J. Phys. Chem. B* **1998**, *102*, 1430.

(40) Mehandru, S. P.; Anderson, A. B. *J. Am. Chem. Soc.* **1988**, *110*, 2061.

(41) In simple terms, the oxidation state of Mo in the oxides (formal charge +6) is much larger than that of Ni or Co (formal charge +2), making difficult the formation of Mo−H bonds or the donation of electrons from Mo into the antibonding $1\sigma_u$ orbital of H_2.

(42) To determine the ΔE of reacion 1, we used the calculated total energies for H_2, H_2O, the bare cluster ($Ni_3Mo_3O_{13}$/$cNi_9cMo_9cO_{35}$, $Co_3Mo_3O_{13}$/$cCo_9cMo_9cO_{35}$, or Mo_4O_{13}/$cMo_{16}cO_{47}$), and the cluster minus the O atom labeled "1" in Figure 6. The structure of the cluster was not allowed to relax after removing the O_1 atom.

(43) This can be expected. During the reduction of bulk $NiMoO_4$, $CoMoO_4$, and MoO_3, the first O atoms that should be removed are those that are coordinated to two metal atoms joining the chains of octahedra.

(44) (a) Pedley, J. B.; Marshall, E. M. *J. Phys. Chem. Ref. Data* **1984**, *12*, 967. (b) Lide, D. R., Ed. *CRC Handbook of Chemical Physics*, 73rd ed.; CRC Press: Boca Raton, FL, 1992.

(45) Dean, J. A., Ed. *Lange's Handbook of Chemistry*, 13th ed; McGraw-Hill: New York, 1985; Table 9-1.

(46) (a) On the oxide clusters, the relative strength of the Ni−H and Co−H bonds varies in a way similar to trends observed for the heat of adsorption of H_2 on the pure metals: Co < Ni.[46b] Since the oxidation state of these elements in the oxide clusters is similar (formal charge +2), the differences in Tables 1 and 2 reflect differences in the intrinsic chemical activity of Co and Ni. (b) Somorjai, G. A. *Introduction to Surface Chemistry and Catalysis*; Wiley: New York, 1994; p 312.

(47) (a) Bartholomew, C. H.; Agrawal, P. K.; Katzer, J. R. *Adv. Catal.* **1982**, *31*, 135. (b) Oudar, J.; Wise, H., Eds. *Deactivation and Poisoning of Catalysts*; Marcel Dekker: New York, 1991.

(48) Muryn, C. A.; Purdie, D.; Hardman, P.; Johnson, A. L.; Prakash, N. S.; Raikar, G. N.; Thorton, G.; Law, D. S. *Faraday Discuss. Chem. Soc.* **1990**, *89*, 77.

(49) (a) Vairavamurthy, A.; Manowitz, B.; Luther, G. W.; Jeon, Y. *Geochim. Cosmochim. Acta* **1993**, *57*, 1619. (b) Morra, M. J.; Fendorf, S. E.; Brown, P. D. *Geochim. Cosmochim. Acta* **1997**, *61*, 683. (c) Frank, F.; Hedman, B.; Carlson, R. M. K.; Tyson, T. A.; Roe, A. L.; Hodgson, K. O. *Biochemistry* **1987**, *26*, 4975. (d) George, G. N.; Gorbaty, M. L. *J. Am. Chem. Soc.* **1989**, *111*, 3182.

(50) Chaturvedi, S.; Rodriguez, J. A.; Brito, J. L. *Catal. Lett.* **1998**, *51*, 85.

(51) Arnoldy, P.; van den Heijkant, J. A. M.; de Bock, G. D.; Moulijn, J. A. *J. Catal.* **1985**, *92*, 35.

(52) (a) Lin, J.; May, J. A.; Didziulis, S. V.; Solomon, E. I. *J. Am. Chem. Soc.* **1992**, *114*, 4718. (b) Casarin, M.; Maccato, C.; Tondello, E.; Vittadini, A. *Surf. Sci.* **1995**, *343*, 115. (c) Casarin, M.; Maccato, C.; Vittadini, A. *Surf. Sci.* **1997**, *377*−*379*, 587.

(53) Wilkinson, G., Willard, R. D., McCleverty, R. D., Eds. *Comprehensive Coordination Chemistry*; Pergamon Press: New York, 1987; Chapters 16, 36, and 50.

(54) (a) Brauman, J. I.; Smyth, K. C. *J. Am. Chem. Soc.* **1969**, *91*, 7778. (b) Steiner, B. *J. Chem. Phys.* **1968**, *49*, 5097.

(55) Moeller, T. *Inorganic Chemistry*; Wiley: New York, 1982; p 81.

(56) Rodriguez, J. A. *Surf. Sci.* **1992**, *278*, 326.

(57) (a) The charges were calculated using a Mulliken population analysis.[57b] Due to the approximations in this type of approach,[57c] we focus our attention only on relative values and general trends. (b) Mulliken, R. S. *J. Chem. Phys.* **1955**, *23*, 1841. (c) Szabo, A.; Ostlund, N. S. *Modern Quantum Chemistry*; McGraw-Hill: New York, 1989.

(58) PDF No. 24-515. JCPDS Powder Diffraction File, International Centre for Diffraction Data, Swarthmore, PA, 1989.

(59) Courtine, P.; Cord, P. P.; Pannetier, G.; Daumas, J. C.; Montarnal, R. *Bull. Soc. Chim.* **1968**, *12*, 4816.